Charge-exchange reactions on double-β decaying nuclei populating $J^\pi = 2^-$ states

D. Frekers,[1] M. Alanssari,[1] H. Ejiri,[2,3] M. Holl,[1] A. Poves,[4] and J. Suhonen[5]

[1]*Institut für Kernphysik, Westfälische Wilhelms-Universität D-48149 Münster, Germany*
[2]*Research Center for Nuclear Physics, Osaka University, Ibaraki, Osaka 567-0047, Japan*
[3]*Nuclear Physics, Czech Technical University, Prague, Czech Republic*
[4]*Departamento de Fisica Teóretica and IFT-UAM/CSIC, Universidad Autónoma de Madrid, E-28049 Madrid, Spain*
[5]*University of Jyvaskyla, Department of Physics, FI-40014, Finland*

The (^{3}He,t) charge-exchange reaction populating $J^\pi = 2^-$ states has been examined at 420 MeV incident energy for a series of double-β decaying nuclei, i.e., ^{76}Ge, ^{82}Se, ^{96}Zr, ^{100}Mo, ^{128}Te, ^{130}Te, and ^{136}Xe. The measurements were carried out at the Grand Raiden spectrometer of the Research Center for Nuclear Physics at the University Osaka with typical spectral resolution of 30–40 keV. It is found that the charge-exchange reaction leading to 2^- spin-dipole states is selective to the $\sigma\tau$ part of the interaction much similar to the observed selectivity to Gamow-Teller transitions. In the present case, the $\Delta L = 1$ peak cross sections at finite momentum transfers are used to extract the spin-isospin part of the low-lying transition strength near the Fermi surface (i.e., $E_x \leqslant 5$ MeV). Relative strength values are confronted with various model calculations, i.e., the interacting shell model, the quasiparticle random-phase approximation, and the Fermi surface quasiparticle model. The impact on the nuclear matrix elements for the neutrinoless double-β decay is discussed.

I. INTRODUCTION

Charge-exchange reactions at intermediate energies continue to play an important role in many fields of nuclear structure physics. At low momentum transfers, (n,p)- and (p,n)-type reactions selectively induce $\Delta L = 0, \Delta S = 1$ Gamow-Teller (GT) transitions [1–3], and these directly relate to weak interaction properties. Especially for the understanding of the nuclear physics part of $\beta\beta$ decay, the virtues of charge-exchange reactions have been demonstrated in many high-resolution studies using the (^{3}He,t) and the (d,^{2}He) reactions as a probe [4–17]. Following these, we focus in the present study on the extraction of the $\Delta L = 1, \Delta S = 1$, $J^\pi = 2^-$ spin-dipole strength. Here the key nuclei are the $\beta\beta$-decay nuclei ^{76}Ge, ^{82}Se, ^{96}Zr, ^{100}Mo, ^{128}Te, ^{130}Te, and ^{136}Xe, where the spin-dipole strength in the low-energy region, i.e., near the Fermi surface, is investigated, as these transitions mirror ground-state properties of the nuclei in question. One may also notice that in the context of $\beta\beta$ decay, the nuclear matrix element from the spin-dipole transition operator constitutes a significant fraction of the total nuclear matrix element for the neutrinoless ($0\nu\beta\beta$) decay [18,19], and since little is known about the spin-dipole strength from the experimental side, the present study can be associated with the general description of this decay and help reducing the rather disconcerting divergence of the many nuclear structure models, which presently exist [20].

The (^{3}He,t) charge-exchange experiments were performed at the Research Center for Nuclear Physics (RCNP) in Osaka with a 420-MeV ^{3}He beam and using the Grand Raiden spectrometer setup in high-resolution mode [21–25]. Details have already been described in Refs. [7–11,17].

II. SPIN-DIPOLE TRANSITIONS IN CHARGE-EXCHANGE REACTIONS

A. General considerations

The relation between cross section and spin-dipole strength has not yet been established by a rigorous comparison with β-decay data, which is quite contrary to the case of GT transitions. Although several unique first-forbidden β^+ decays and many more for the β^- decays leading to stable daughter nuclei exist, the spectral resolution of previous (p,n)-type and (n,p)-type charge-exchange reactions have so far been insufficient to isolate these transitions. A rather seminal work to study spin-dipole transitions with charge-exchange reactions appears in Ref. [26], where the authors used the (p,n) and (n,p) probes on ^{90}Zr to extract the neutron skin thickness from the total spin-dipole strength. However, a detailed level structure of the low-energy excitation near the Fermi surface could not be identified. The high-resolution (^{3}He,t) reaction reported in this work therefore offers a new window to study these transitions in much greater detail.

In charge-exchange reactions at typical intermediate energies of 100–300 MeV/A the $\Delta L = 1, \Delta S = 1$ transitions to $J^\pi = 2^-$ final states can easily be identified by their characteristic angular distributions. They show a steep rise from zero degrees to the maximum cross section at some finite angle given by the momentum transfer, followed by a steep fall-off again. At angles of maximum cross section the momentum transfer q is typically in the order $q \approx 0.25$ fm^{-1}, thereby leading to an angular momentum $qR \approx 1$. In this kinematic region the $V_{\sigma\tau}$ part of the effective interaction is still the dominating contribution [27–30]. For even-even, $J^\pi = 0^+$ nuclei one can therefore expect selective excitation of $\Delta L = 1$

transitions leading to $J^\pi = 2^-$ states, similar to what is known for $\Delta L = 0$ GT transitions leading to 1^+ states. One may note that $\Delta L = 1$ and $\Delta S = 1$ can also couple to $J^\pi = 0^-$ and $J^\pi = 1^-$; however, these transitions are usually suppressed. This holds in particular for $0^+ \to 0^-$ transitions, which are entirely forbidden at $q = 0$, as they violate time invariance. Further, in charge-exchange reactions it is known that GT transitions to 1^+ final states can be contaminated with $\Delta L = 2$ non-GT components. Similarly for spin-dipole transitions to 2^- final states, $\Delta L = 3$ transitions can contribute.

Following these arguments, one can pursue the extraction of the $\Delta L = 1$ spin-dipole strength in a model-independent way by using the same procedure one usually applies for the extraction of GT strength. However, unlike the GT operator, the isovector spin-dipole transition operator contains a radial dependence, which makes the transition strength dependent on the underlying model wave function. Since in this paper we will be dealing with the integrated spin-dipole strength near the Fermi surface, one can use the radial extent of the nucleus as an average normalization scale for the cross section of the transition. This is similar to what is known for the differential cross section of Coulomb excitation, where the radial extent is a measure of the charge distribution. Near $qR \approx 1$ the relation between charge-exchange cross section and isovector spin-dipole strength may then be written in common notation as

$$\left.\frac{d\sigma^{\mathrm{SD}}}{d\Omega}\right|_{q_{\max}} = \left[\frac{\mu}{\pi\hbar^2}\right]^2 \frac{k_f}{k_i} N_D^{\sigma\tau} \left|\frac{J_{\sigma\tau}^{q_{\max}}}{r_0 A^{1/3}}\right|^2 K_\sigma(M2). \quad (1)$$

Here $J_{\sigma\tau}^{q_{\max}}$ is the volume integral of the $\sigma\tau$ nucleon-nucleon interaction [27–30] at a momentum transfer given by the maximum cross section. In the present case, we have used a value of $J_{\sigma\tau}^{q_{\max}} = 145$ MeV fm^3 and $r_0 = 1.25$ fm. The distortion factor $N_D^{\sigma\tau}$ can be readily taken from an eikonal approximation, i.e.,

$$N_D^{\sigma\tau} = \exp(aA^{1/3} + b) \quad (2)$$

with $a = -0.895$ and $b = 1$ (see, e.g., Refs. [2,31–33]). The relative strength factor $K_\sigma(M2)$ connects to the transition operator $M2$ via

$$K_\sigma(M2) \propto |M2|^2 \quad (3)$$

with

$$M2 = \langle f \| \tau^- [\sigma \times rY_1]_2 \| i \rangle. \quad (4)$$

The value of the proportionality constant in Eq. (3) has not been established yet; however, in this paper we will show that there is evidence for a universal proportionality, once the kinematic and reaction specific quantities are separated from the cross-section formula in Eq. (1). Unfortunately, there are only a few log-ft values for first-order unique forbidden β^+ decays to stable nuclei known. They all range between 9.1 and 9.9, yet for none of them high-resolution charge-exchange data exist. Therefore, a program to establish the above-quoted connection between weak decays and hadronic charge-exchange reactions is highly warranted, and for some key nuclei, i.e., ^{74}Ge, ^{122}Sn, ^{116}Cd, and ^{124}Te, such a program is presently active at RCNP [34].

B. Experimental situation

In Fig. 1 are shown a series of low-energy excitation spectra for (^{3}He,t) reactions on $\beta\beta$ decaying nuclei ranging from $A = 76$ to 136, where spin dipole transitions are indicated. The 0° and the 2.5° spectra are overlaid to show the angular distribution effect, since GT transitions peak at zero degree, and the spin dipole transitions to 2^- states at around 2° (note that the excitation energies for the $J^\pi = 2^-$ final states are bold faced in the spectra). From these spectra, one can already qualitatively recognize a general trend from rather weak transitions at $A \leqslant 100$ to comparatively strong transitions when approaching $A = 136$. The most spectacular situation is encountered for ^{136}Xe, where the spin-dipole transition of the single state at 0.995 MeV is by far the strongest transition in these spectra. It is also worth mentioning that the low-lying spin-dipole transitions exhibit no sizable fragmentation, which is contrary to GT transition. Especially for the ^{76}Ge case, where the level of fragmentation for GT transitions is exceedingly high, a fact which has been attributed to collective surface degrees of freedom [8,35–37], there are only two clearly identifiable 2^- states below 5 MeV excitation. A more refined analysis of angular distributions of individual states, which included a multipole decomposition in cases of unresolved states, i.e., those which were masked by 1^+ states, revealed in total seven 2^- states for the ^{76}Ge case, four for the ^{82}Se case, one for the ^{96}Zr case, two for the ^{100}Mo case, two (respectively four) for the cases ^{128}Te (^{130}Te), and one 2^- state for the ^{136}Xe case (cf. Table I).

In Fig. 2 angular distributions for the lowest-lying 2^- states in the various $\beta\beta$ decaying systems are presented. They exhibit in all cases the characteristic shape for a spin-dipole transition. Distorted-wave (DW) calculations were performed to describe the cross-section angular distributions, which were carried out in the same way as, for instance, described in Refs. [8,33] using the code FOLD [38] and the Love-Franey nucleon-nucleon interactions [29]. Single-particle wave functions were generated in a Woods-Saxon potential with a radius of $r_0 = 1.25$ fm, and transition amplitudes were derived from the code NORMOD [39]. Similar to GT transitions, the shape of the angular distributions is quite robust against changes of the single-particle wave functions within reasonable bounds. In order to get a good agreement with the data, a $\Delta L = 3$ contribution was needed in all cases, as indicated in the figure.

From those angular distributions which exhibited a significant spin-dipole strength, the maximum cross section for the spin-dipole transition was extracted and the relative strength $K_\sigma(M2)$ determined according to Eq. (1). The various quantities are summarized in Table I together with the integrated strength from 0 to 5 MeV excitation. Although the analysis covered an excitation energy up to 5 MeV, one finds that in most cases the 2^- states are located significantly below 2 MeV. Table I lists states which are fully resolved and those which required a multipole decomposition consisting of the two major components $\Delta L = 0$ and $\Delta L = 1$. These latter states are indicated as masked, and their relative transition strength carries each an uncorrelated systematic error, which we conservatively estimate at 15%. The errors of the resolved states are determined by the $K_\sigma(M2)$ extraction routine and are
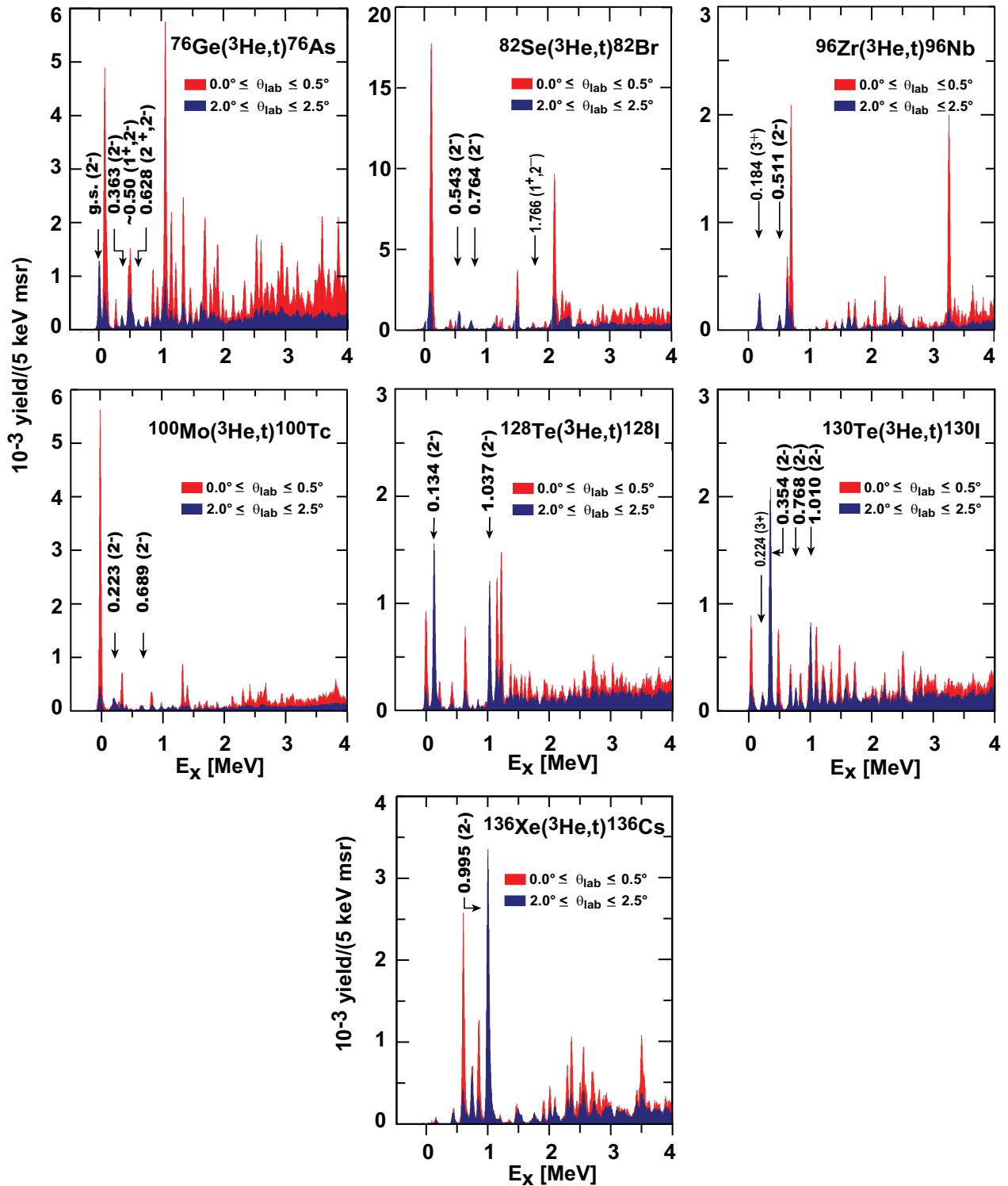
FIG. 1. Low-energy excitation spectra obtained from (^{3}He,t) charge-exchange reaction on seven $\beta\beta$ decaying nuclei. The spectra for the scattering angle intervals [0–0.5°] (in red) and [2–2.5°] (in blue) are overlaid to visualize the angular distribution effect of GT and spin-dipole transitions. Excitation energies are indicated for the most clearly visible 2$^-$ transitions. The search for 2$^-$ states was extended to 5 MeV, but no isolated 2$^-$ states were observed even above 4 MeV in any of these nuclei. For a complete analysis of GT transitions, one may refer to Refs. [7–11,17].

typically around 7%. The individual error values are added in quadrature and appear only as combined errors for the summed strengths in Table I.

When adding the individual strength values, one can of course not rule out that extremely weak transitions have evaded detection. However, in the present carefully conducted analysis

TABLE I. Compilation of low-lying ($E_x \leqslant 5$ MeV) $J^\pi = 2^-$ states and their relative transition strengths $K_\sigma(M2)$ populated by the $(^3\text{He},t)$ charge-exchange reaction on various $\beta\beta$ decaying nuclei. A number of unresolved 2^- states appear in the spectra as rather weak transitions as indicated in the last column. Their strength was extracted by a multipole decomposition consisting of the two major components, $\Delta L = 0$ and $\Delta L = 1$.

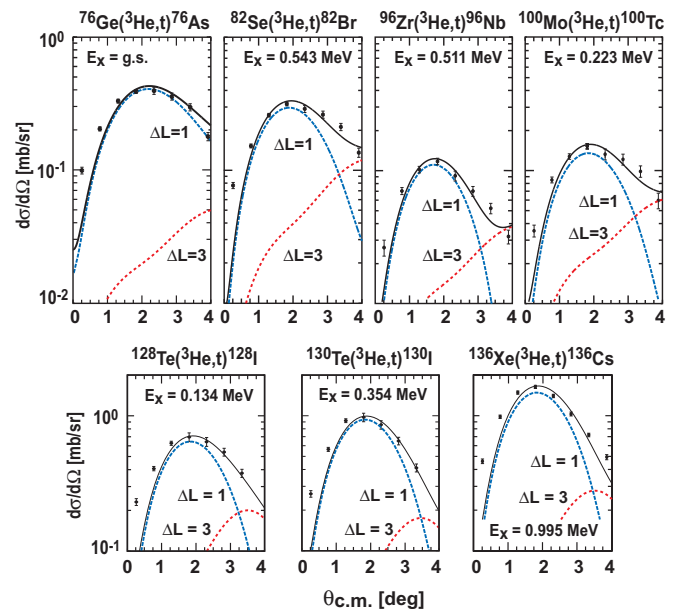| Reaction	E_x [MeV]	$\frac{d\sigma^{SD}}{d\Omega}\big|_{q_{max}}$ [mb/sr]	$K_\sigma(M2)$ [fm^2]	Comment
$^{76}\text{Ge}(^3\text{He},t)^{76}\text{As}$	0	0.40	1.8	Resolved
	0.363	0.064	0.28	Resolved
	0.500	0.13	0.58	Masked
	1.573	0.024	0.1	Masked
	1.929	0.016	0.07	Masked
	3.134	0.022	0.1	Masked
	3.190	0.03	0.13	Masked
$\sum K_\sigma(M2)$			3.06(16)	
$^{82}\text{Se}(^3\text{He},t)^{82}\text{Kr}$	0.543	0.30	1.54	Resolved
	0.764	0.16	0.84	Resolved
	1.680	0.041	0.21	Masked
	1.766	0.05	0.26	Masked
$\sum K_\sigma(M2)$			2.84(14)	
$^{96}\text{Zr}(^3\text{He},t)^{96}\text{Mo}$	0.511	0.12	0.84	Resolved
$\sum K_\sigma(M2)$			0.84(6)	
$^{100}\text{Mo}(^3\text{He},t)^{100}\text{Ru}$	0.223	0.141	1.06	Resolved
	0.689	0.048	0.37	Resolved
$\sum K_\sigma(M2)$			1.43(8)	
$^{128}\text{Te}(^3\text{He},t)^{128}\text{Xe}$	0.134	0.67	8.4	Resolved
	1.037	0.56	7.0	Resolved
$\sum K_\sigma(M2)$			15.4(8)	
$^{130}\text{Te}(^3\text{He},t)^{130}\text{Xe}$	0.345	0.95	12.3	Resolved
	0.768	0.097	1.26	Resolved
	1.010	0.33	4.28	Resolved
	1.216	0.08	1.04	Masked
$\sum K_\sigma(M2)$			18.9(10)	
$^{136}\text{Xe}(^3\text{He},t)^{136}\text{Cs}$	0.995	1.53	21.9	Resolved
$\sum K_\sigma(M2)$			21.9(16)	

FIG. 2. Cross-section angular distributions for the lowest-lying 2^- states in various $\beta\beta$ decaying nuclei. The solid lines are DW calculations for the sum of the $\Delta L = 1$ and $\Delta L = 3$ transitions as described in the text. The dotted lines show these transitions separately.

shell to a proton in a half-empty $\pi g_{7/2}$ shell, whereby a comparatively large transition strength can be expected within a single state near the Fermi surface. A similar situation is encountered for the two tellurium isotopes. The higher $\nu h_{11/2}$ occupancy due to the extra two neutrons in the $\nu d_{3/2}$ shell should also make the spin-dipole transition strength larger for ^{130}Te than for ^{128}Te. This expectation is indeed verified by the experiment (cf. Fig. 3). In the ^{96}Zr and ^{100}Mo cases the $(2p1f)$
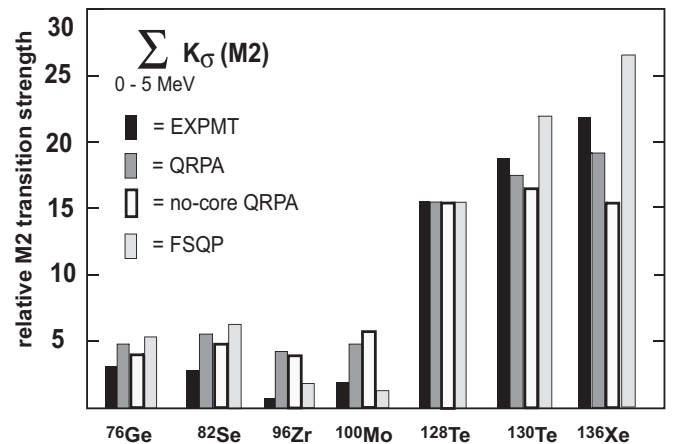

FIG. 3. Comparison of the relative spin-dipole excitation strengths for the $A = 76, 96, 100, 128, 130,$ and 136 systems. The black bars indicate the experimental values from the $(^3\text{He},t)$ charge-exchange reactions on the $\beta\beta$ decaying nuclei indicated on the lower axis. All theoretical values have been scaled in order to have the values for ^{128}Te match the experimental one. This is for presentation purposes to show the general trend. Absolute numbers appear in Table III.

their contributions cannot conceivably add up to more than a few percent in total and thereby cannot change the general A-dependent trend.

III. EVALUATING THE SPIN-DIPOLE STRENGTH NEAR THE FERMI SURFACE

The integrated spin-dipole strengths for the seven $\beta\beta$ decaying nuclei, as they appear in Table I, have been plotted in Fig. 3 and compared with theoretical model predictions, i.e., the proton-neutron quasiparticle random-phase approximation (pnQRPA) and the Fermi surface quasiparticle model (FSQP).

Starting with a simple shell model, of which an illustration is given in Fig. 4, the global features are already qualitatively accounted for. In ^{136}Xe, a $\Delta L = 1$ charge-exchange transition requires promoting a neutron from a fully occupied $\nu h_{11/2}$
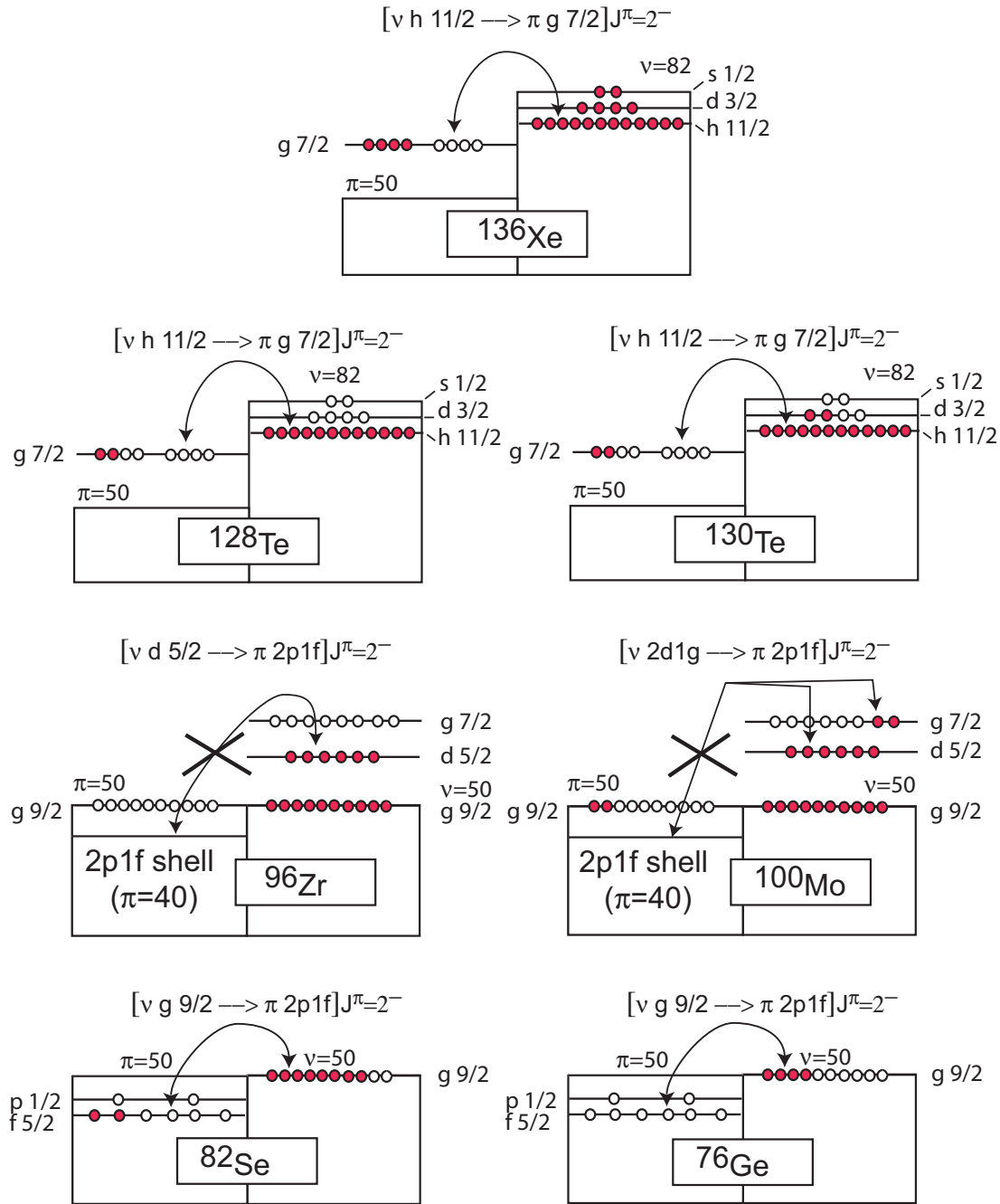
FIG. 4. Sketch of shell-model configurations near the Fermi surface showing $n \rightarrow p$ transitions for $\Delta L = 1$ in (p,n)-type charge-exchange reactions leading to $J^{\pi} = 2^{-}$ states in the daughter nucleus. Full circles indicate occupied configurations, and open circles indicate vacant configurations.

proton shell is blocked and transitions from the $\nu d_{5/2}$ and $\nu g_{7/2}$ configurations are not possible. Thus, in the pure shell-model case, low-lying $\Delta L = 1$ transitions to 2^{-} states cannot occur. This extreme situation is then relaxed again for ^{76}Ge and ^{82}Se (cf. Fig. 4).

A. Interacting shell model (ISM)

A more realistic situation is given by large-scale calculations in the framework of the ISM, which calculates shell-model occupancies near the Fermi surface. These calculations have been performed in Ref. [40] for a series of $\beta\beta$-decay nuclei including those which are the subject of the present study. In Table II are listed the various proton and neutron shell-model occupancies from these calculations. Since the absolute spin-dipole strength cannot easily be calculated within the ISM, we therefore compare the occupation numbers from the ISM with those from a QRPA calculation described in the next section.

TABLE II. Compilation of shell-model occupation numbers for various $\beta\beta$ decaying nuclei as evaluated by the ISM and the pnQRPA. The ISM numbers for ^{100}Mo have not been calculated.

	ISM	QRPA		ISM	QRPA		ISM	QRPA		ISM	QRPA		ISM	QRPA
			$\nu0g_{9/2}$	6.39	4.61	$\nu0f_{5/2}$	4.79	5.51	$\nu1p_{3/2}$	3.55	3.84	$\nu1p_{1/2}$	1.27	1.81
^{76}Ge			$\pi0g_{9/2}$	0.66	0.27	$\pi0f_{5/2}$	2.00	1.66	$\pi1p_{3/2}$	0.99	2.10	$\pi1p_{1/2}$	0.35	0.20
			$\nu0g_{9/2}$	8.30	8.04	$\nu0f_{5/2}$	5.88	5.81	$\nu1p_{3/2}$	3.93	3.93	$\nu1p_{1/2}$	1.89	1.92
^{82}Se			$\pi0g_{9/2}$	0.52	0.36	$\pi0f_{5/2}$	3.34	2.97	$\pi1p_{3/2}$	1.79	2.58	$\pi1p_{1/2}$	0.35	0.28
	$\nu0h_{11/2}$ 0.23	0.09	$\nu0g_{7/2}$ 0.15	0.59		$\nu1d_{5/2}$ 5.36	5.09	$\nu1d_{3/2}$ 0.15	0.14	$\nu2s_{1/2}$ 0.11	0.16				
^{96}Zr	$\pi0g_{9/2}$ 0.75	1.79	$\pi0f_{5/2}$ 5.70	5.44		$\pi1p_{3/2}$ 3.73	3.62	$\pi1p_{1/2}$ 1.82	1.17						
	$\nu0h_{11/2}$	0.39	$\nu0g_{7/2}$	2.32		$\nu1d_{5/2}$	4.69	$\nu1d_{3/2}$	0.41	$\nu2s_{1/2}$	0.4			
^{100}Mo	$\pi0g_{9/2}$	3.67	$\pi0f_{5/2}$	5.35		$\pi1p_{3/2}$	3.57	$\pi1p_{1/2}$	1.35						
	$\nu0h_{11/2}$ 8.74	7.53	$\nu0g_{7/2}$ 7.50	7.50		$\nu1d_{5/2}$ 5.58	5.75	$\nu1d_{3/2}$ 2.59	3.28	$\nu2s_{1/2}$ 1.59	1.74				
^{128}Te	$\pi0h_{11/2}$ 0.17	0.20	$\pi0g_{7/2}$ 1.18	1.08		$\pi1d_{5/2}$ 0.43	0.78	$\pi1d_{3/2}$ 0.19	0.05	$\pi2s_{1/2}$ 0.05	0.02				
	$\nu0h_{11/2}$ 9.93	8.92	$\nu0g_{7/2}$ 7.69	7.67		$\nu1d_{5/2}$ 5.71	5.84	$\nu1d_{3/2}$ 2.95	3.54	$\nu2s_{1/2}$ 1.72	1.83				
^{130}Te	$\pi0h_{11/2}$ 0.16	0.18	$\pi0g_{7/2}$ 1.31	1.14		$\pi1d_{5/2}$ 0.36	0.73	$\pi1d_{3/2}$ 0.13	0.04	$\pi2s_{1/2}$ 0.03	0.01				
	$\nu0h_{11/2}$ 12	12	$\nu0g_{7/2}$ 8	8		$\nu1d_{5/2}$ 6	6	$\nu1d_{3/2}$ 4	4	$\nu2s_{1/2}$ 2	2				
^{136}Xe	$\pi0h_{11/2}$ 0.37	0.37	$\pi0g_{7/2}$ 2.72	2.48		$\pi1d_{5/2}$ 0.79	1.22	$\pi1d_{3/2}$ 0.10	0.08	$\pi2s_{1/2}$ 0.03	0.03				

B. Proton-neutron QRPA

A proton-neutron QRPA (pnQRPA) calculation allows evaluating the low-energy spin-dipole strength distributions and thereby establishing a direct comparison with the experimental data. The present calculations were performed with a G-matrix-based two-body interaction [41], and the necessary quasiparticle energies and occupancies were produced by solving the BCS equations. The pairing strengths for protons and neutrons were adjusted to reproduce the phenomenological proton and neutron pairing gaps in a given single-particle model space [42,43]. The resulting occupancies near the proton and neutron Fermi surfaces are listed in Table II side by side with the values from the ISM calculations.

The single-particle energies of the nuclear mean field were extracted from a Coulomb-corrected Woods-Saxon potential with the Bohr-Mottelson parametrization [44], suitable for nuclei lying close to the stability line. For the present comparison with the experiment, only the low-energy ($E_x < 5$ MeV) spin-dipole strength was taken into account. The relative values, once scaled to the experimental ^{128}Te value, are shown in Fig. 3. The calculated low-energy absolute strength values are listed in Table III.

The pnQRPA calculations were performed in a single-particle-model space spanning at least one oscillator shell below and one above the proton and neutron Fermi surface. The model space was extended in the no-core QRPA calculations

TABLE III. Comparison of summed low-lying spin-dipole strength from different models. The summed strength was computed for excitation energies $E_x < 5$ MeV. Column 3 shows the strength for the QRPA calculations and column 4 shows the results for the no-core QRPA calculations. Column 5 shows the experimental relative strengths extracted from cross-section data according to Eq. (1).

Nucl.	FSQP [fm^2]	QRPA [fm^2]	No-core QRPA [fm^2]	$K_\sigma(M2)$ [fm^2]
^{76}Ge	1.7(4)	5.11	5.76	3.06(16)
^{82}Se	2.0(4)	5.95	6.93	2.84(14)
^{96}Zr	0.6(2)	4.58	5.92	0.84(6)
^{100}Mo	0.44(15)	5.14	8.54	1.43(8)
^{128}Te	4.8(7)	16.28	22.40	15.4(8)
^{130}Te	7.0(11)	18.48	23.87	18.9(10)
^{136}Xe	8.3(12)	20.31	22.46	21.9(16)

to include the core orbitals and many additional higher-lying quasibound orbitals. The results from these calculations are also shown in Fig. 3, and absolute values are also given in Table III.

The pnQRPA as well as the no-core QRPA calculations for the low-excitation spin-dipole strength do not exhibit a strong shell effect near mass $A \approx 100$. There is no significant A dependence among the masses $A \leqslant 100$, and likewise, little to no dependence among the masses $A = 128, 130,$ and 136. This is quite contrary to experimental observation. There are, however, marked differences when comparing the two nuclear-structure models, i.e., QRPA and ISM. These show up in the occupation numbers, where these differences are particularly pronounced for the open-shell nuclei around the masses $A < 100$ and far less near the shell closure at ^{136}Xe (cf. Table II). We note that occupancies of single-particle orbitals play a notable role in the theoretical predictions of $0\nu\beta\beta$-decay rates [45,46]. They also give insight into the differences between models, and since experimental data are now available which these models can be confronted with, it could help generating convergence among the different calculations of $\beta\beta$-decay nuclear matrix elements, which so far has not readily been achieved (see, e.g., Ref [20])

C. Fermi surface quasiparticle model

The Fermi surface quasiparticle model (FSQP) is a semi-microscopic approach to evaluate nuclear matrix elements for single β and $\beta\beta$ decays [5,16,47–49]. The model correlates single β-decay strength values of neighboring nuclei with their proton-neutron occupation amplitudes derived from the quasiparticle model calculations. The FSQP model has been capable of making rather precise predictions for the $2\nu\beta\beta$ nuclear matrix elements for almost all $\beta\beta$ decaying nuclei [5,47,49,50].

In the FSQP model the spin-dipole nuclear matrix element is expressed as

$$M2 = k_{\text{eff}} M2(\text{QP}), \qquad (5)$$

where $M2(\text{QP})$ is the quasiparticle nuclear matrix element and k_{eff} includes all nuclear correlations, as well as non-nucleonic $\sigma\tau$ and nuclear medium effects, all of which are not explicitly included in the quasiparticle model. It is assumed to be a universal factor, which has been evaluated from a study of β-decay properties of numerous neighboring nuclei. A universal value of $k_{\text{eff}} \approx 0.25 \pm 0.04$ is generally accepted [51]. The quasiparticle nuclear matrix element is then expressed in terms of the single-particle nuclear matrix element $M2(\text{SP})$ and a pairing factor P_{np} as

$$M2(\text{QP}) = P_{np} M2(\text{SP}), \qquad (6)$$

where the pairing factor is derived from the proton and neutron occupation (V) and vacancy (U) amplitudes. These are given by the neutron and proton configurations in the relevant orbitals j, j' near the Fermi surface, i.e., $P_{np} = V_n(j)U_p(j')$. The connection to the experimental $(^3\text{He},t)$ cross section for spin-dipole transitions is the same as in Eq. (3), i.e.,

$$K_\sigma(M2) \propto k_{\text{eff}}[P_{np}M2(\text{SP})]^2. \qquad (7)$$

The results from the FSQP model are also displayed in Fig. 3. The shell effects near $A = 100$ are in almost perfect accordance with the experimental findings. Further, the sudden increase of the low-lying spin-dipole strength at and above $A = 128$ also captures the experimental situation remarkably well. In order to judge the level of agreement, one may note that the FSQP values carry an estimated overall uncertainty of $\approx 15\%$ as a result of their determination from experimental data.

IV. FINAL COMPARISON

Table III contains a final comparison of absolute values as they have been calculated by the above-quoted models. The values have also been put into relation to the quantities $K_\sigma(M2)$, which were extracted solely on the basis of Eq. (1). The two QRPA calculations agree with each other as far as the overall magnitude of the low-lying spin-dipole strength is concerned; however, the values are on average about a factor 3–5 larger than in the FSQP calculations.

V. CONCLUSION

It has been shown for the first time that charge-exchange reactions can be used to extract detailed information about the spin-dipole transitions leading to low-lying individual $J^\pi = 2^-$ states in much the same way as has been done for GT transitions in the past. This has been possible because of the unprecedented high resolution, which has been obtained at the Grand Raiden magnetic spectrometer at RCNP, Osaka, using the $(^3\text{He},t)$ charge-exchange reaction at 420 MeV. A complete analysis of low-lying 2^- states for seven $\beta\beta$-decay nuclei ranging from $A = 76$ to $A = 136$ was performed, and some key features of the mass dependent low-excitation spin-dipole strength were unveiled, like the much reduced level of fragmentation when compared to GT transitions or the strong reflection of the underlying shell-model properties on the cross section. The relative transition strength integrated up to 5 MeV excitation was compared with a microscopic shell model, a QRPA, and a semimicroscopic FSQP calculation. All of these had been devised to calculate $\beta\beta$-decay nuclear matrix elements for these nuclei. Some noticeable differences among these models were observed as far as their predictive power for the experimental integrated low-energy spin-dipole strength is concerned. In how far these differences will affect the size of the nuclear matrix elements for $0\nu\beta\beta$ decay remains an issue to be resolved by more theoretical studies. Since spin-dipole transitions are an important part of the $0\nu\beta\beta$ nuclear matrix elements, the present data ought to be an important input when tuning the properties of the nuclear wave functions of the $\beta\beta$ decaying nuclei.

[1] C. D. Goodman, C. A. Goulding, M. B. Greenfield, J. Rapaport, D. E. Bainum, C. C. Foster, W. G. Love, and F. Petrovich, Phys. Rev. Lett. **44**, 1755 (1980).

[2] T. N. Taddeucci, C. A. Goulding, T. A. Carey, R. C. Byrd, C. D. Goodman, C. Gaarde, J. Larsen, D. Horen, J. Rapaport, and E. Sugarbaker, Nucl. Phys. A **469**, 125 (1987).

[3] K. P. Jackson, A. Celler, W. P. Alford, K. Raywood, R. Abegg, R. E. Azuma, C. K. Campbell, S. El-Kateb, D. Frekers, P. W. Green *et al.*, Phys. Lett. B **201**, 25 (1988).

[4] H. Akimune, H. Ejiri, M. Fujiwara, I. Daito, T. Inomata, R. Hazama, A. Tamii, H. Toyokawa, and M. Yosoi, Phys. Lett. B **394**, 23 (1997); **665**, 424 (2008).

[5] H. Ejiri, J. Phys. Soc. Jpn. **78**, 074201 (2009).

[6] E.-W. Grewe, D. Frekers, S. Rakers, T. Adachi, C. Bäumer, N. T. Botha, H. Dohmann, H. Fujita, Y. Fujita, K. Hatanaka *et al.*, Phys. Rev. C **76**, 054307 (2007).

[7] P. Puppe, D. Frekers, T. Adachi, H. Akimune, N. Aoi, B. Bilgier, H. Ejiri, H. Fujita, Y. Fujita, M. Fujiwara *et al.*, Phys. Rev. C **84**, 051305 (2011).

[8] J. H. Thies, D. Frekers, T. Adachi, M. Dozono, H. Ejiri, H. Fujita, Y. Fujita, M. Fujiwara, E.-W. Grewe, K. Hatanaka *et al.*, Phys. Rev. C **86**, 014304 (2012).

[9] J. H. Thies, T. Adachi, M. Dozono, H. Ejiri, D. Frekers, H. Fujita, Y. Fujita, M. Fujiwara, E.-W. Grewe, K. Hatanaka *et al.*, Phys. Rev. C **86**, 044309 (2012).

[10] J. H. Thies, P. Puppe, T. Adachi, M. Dozono, H. Ejiri, D. Frekers, H. Fujita, Y. Fujita, M. Fujiwara, E.-W. Grewe *et al.*, Phys. Rev. C **86**, 054323 (2012).

[11] P. Puppe, A. Lennarz, T. Adachi, H. Akimune, H. Ejiri, D. Frekers, H. Fujita, Y. Fujita, M. Fujiwara, E. Ganioğlu *et al.*, Phys. Rev. C **86**, 044603 (2012).

[12] E.-W. Grewe, C. Bäumer, H. Dohmann, D. Frekers, M. N. Harakeh, S. Hollstein, H. Johansson, K. Langanke, G. Martínez-Pinedo, F. Nowacki *et al.*, Phys. Rev. C **77**, 064303 (2008).

[13] E.-W. Grewe, C. Bäumer, H. Dohmann, D. Frekers, M. N. Harakeh, S. Hollstein, H. Johansson, L. Popescu, S. Rakers, D. Savran *et al.*, Phys. Rev. C **78**, 044301 (2008).

[14] H. Dohmann, C. Bäumer, D. Frekers, E.-W. Grewe, M. N. Harakeh, S. Hollstein, H. Johansson, L. Popescu, S. Rakers, D. Savran *et al.*, Phys. Rev. C **78**, 041602 (2008).

[15] H. Ejiri, Phys. Rep. **338**, 265 (2000).

[16] H. Ejiri, J. Phys. Soc. Jpn. **74**, 2101 (2005).

[17] D. Frekers, M. Alanssari, T. Adachi, B. T. Cleveland, M. Dozono, H. Ejiri, S. R. Elliott, H. Fujita, Y. Fujita, M. Fujiwara *et al.*, Phys. Rev. C **94**, 014614 (2016).

[18] O. Civitarese and J. Suhonen, Phys. Lett. B **626**, 80 (2005).

[19] J. Hyvärinen and J. Suhonen, Adv. High Energy Phys. **2016**, ID 4714829 (2016).

[20] P. Vogel, J. Phys. G: Nucl. Part. Phys. **39**, 124002 (2012).

[21] T. Wakasa, K. Hatanaka, Y. Fujita, G. P. A. Berg, H. Fujimura, H. Fujita, M. Itoh, J. Kamiya, T. Kawabata, K. Nagayama *et al.*, Nucl. Instrum. Methods Phys. Res. A **482**, 79 (2002).

[22] M. Fujiwara, H. Akimune, I. Daito, H. Fujimura, Y. Fujita, H. Hatanaka, H. Ikegami, I. Katayama, K. Nagayama, N. Matsuoka *et al.*, Nucl. Instrum. Methods Phys. Res. A **422**, 484 (1999).

[23] Y. Fujita, K. Hatanaka, G. P. A. Berg, K. Hosono, N. Matsuoka *et al.*, Nucl. Instrum. Methods Phys. Res. B **126**, 274 (1997).

[24] H. Fujita, G. P. A. Berg, Y. Fujita, K. Hatanaka, T. Noro, E. J. Stephenson, C. C. Foster, H. Sakaguchi, M. Itoh, T. Taki *et al.*, Nucl. Instrum. Methods Phys. Res. A **469**, 55 (2001).

[25] H. Fujita, Y. Fujita, G. P. A. Berg, A. D. Bacher, C. C. Foster, K. Hara, K. Hatanaka, T. Kawabata, T. Noro, H. Sakaguchi *et al.*, Nucl. Instrum. Methods Phys. Res. A **484**, 17 (2002).

[26] K. Yako, H. Sagawa, and H. Sakai, Phys. Rev. C **74**, 051303(R) (2006).

[27] W. G. Love and M. A. Franey, Phys. Rev. C **24**, 1073 (1981).

[28] W. G. Love, *Spin Excitations in Nuclei*, edited by F. Petrovich, G. E. Brown, G. T. Garvey, C. D. Goodman, R. A. Lindgren, and W. G. Love (Plenum Press, New York, 1982), pp. 205–232.

[29] M. A. Franey and W. G. Love, Phys. Rev. C **31**, 488 (1985).

[30] W. G. Love, A. Klein, M. A. Franey, and K. Nakayama, Can. J. Phys. **65**, 536 (1987).

[31] R. G. T. Zegers (private communication).

[32] G. Perdikakis, R. G. T. Zegers, Sam M. Austin, D. Bazin, C. Caesar, J. M. Deaven, A. Gade, D. Galaviz, G. F. Grinyer, C. J. Guess *et al.*, Phys. Rev. C **83**, 054614 (2011).

[33] D. Frekers, P. Puppe, J. H. Thies, and H. Ejiri, Nucl. Phys. A **916**, 219 (2013).

[34] H. Akimune, H. Ejiri, D. Frekers, and M. Harakeh, Research Center Nuclear Physics (RCNP), Osaka University, Research Proposal E425 (2014).

[35] P. Sarriguren, E. Moya de Guerra, and A. Escuderos, Nucl. Phys A **691**, 631 (2001).

[36] P. Sarriguren, E. Moya de Guerra, and A. Escuderos, Phys. Rev. C **64**, 064306 (2001).

[37] P. Sarriguren, E. Moya de Guerra, L. Pacearescu, A. Faessler, F. Šimkovic, and A. A. Raduta, Phys. Rev. C **67**, 044313 (2003).

[38] J. Cook and J. A. Carr, computer program FOLD, Florida State University, 1988 (unpublished); based on F. Petrovich and D. Stanley, Nucl. Phys. A **275**, 487 (1977); modified as described in J. Cook, K. W. Kemper, P. V. Drumm, L. K. Fifield, M. A. C. Hotchkis, T. R. Ophel, and C. L. Woods, Phys. Rev. C **30**, 1538 (1984); R. G. T. Zegers, S. Fracasso and G. Colò, NSCL, Michigan State University, 2006 (unpublished).

[39] M. A. Hofstee, S. Y. van der Werf, A. M. van den Berg, N. Blasi, J.A. Bordewijk, W. T. A. Borghols, R. De Leo, G. T. Emery, S. Fortier, S. Galès *et al.*, Nucl. Phys. A **588**, 729 (1995).

[40] E. Caurier, J. Menéndez, F. Nowacki, and A. Poves, Phys. Rev. Lett. **100**, 052503 (2008).

[41] K. Holinde, Phys. Rep. **68**, 121 (1981).

[42] J. Suhonen, A. Faessler, T. Taigel, and T. Tomoda, Phys. Lett. B **202**, 174 (1988).

[43] J. Suhonen, Nucl. Phys. A **563**, 205 (1993).

[44] A. Bohr and B. Mottelson, *Nuclear Structure* (Benjamin, New York, 1969).

[45] J. Suhonen and O. Civitarese, Nucl. Phys. A **847**, 207 (2010).

[46] J. Suhonen, Nucl. Phys. A **853**, 36 (2011).

[47] H. Ejiri, J. Phys. Soc. Jpn. **81**, 033201 (2012).

[48] H. Ejiri, AIP Conf. Proc. **1572**, 40 (2013).

[49] H. Ejiri and D. Frekers, J. Phys. G: Nucl. Part. Phys. **43**, 11LT01 (2016).

[50] J. Vergados, H. Ejiri, and F. Šimkovic, Rep. Prog. Phys. **75**, 106301 (2012).

[51] H. Ejiri, N. Soukouti, and J. Suhonen, Phys. Lett. B **729**, 27 (2014).